Available online at www.sciencedirect.com

ScienceDirect

Ceramics International 40 (2014) 523–529

CERAMICS INTERNATIONAL

www.elsevier.com/locate/ceramint

Effects of rare-earth (Er, La and Yb) doping on morphology and structure properties of ZnO nanostructures prepared by wet chemical method

Reza Zamiri[a,*], A.F. Lemos[a], Avito Reblo[a], Hossein Abbastabar Ahangar[b], J.M.F. Ferreira[a]

[a]Department of Materials Engineering and Ceramic,University of Aveiro, Campus Santiago, 3810-193 Aveiro, Portugal
[b]Islamic Azad University, Najafabad Branch, Faculty of Science, Isfahan, Iran

Received 17 April 2013; received in revised form 3 June 2013; accepted 4 June 2013
Available online 17 June 2013

Abstract

Rare-earth (Er, La and Yb) doped ZnO nanostructures have been synthesized by precipitation. The prepared samples were characterized by X-ray diffraction (XRD), scanning electron microscopy (SEM), and energy-dispersive X-ray spectroscopy (EDS). Their optical properties were studied by Raman spectroscopy at room temperature and UV–Visible diffuse reflectance spectroscopy techniques. The effects of rare-earth dopant on morphology and optical properties of the prepared materials were studied and discussed. It was found that the presence of rare-earth ion in crystal structure of ZnO can change the morphology and band gap of ZnO nanostructures.

Keywords: D. ZnO; Nanostructured materials; Rare earth

1. Introduction

Semiconductor quantum dots (QDs) with unique optoelectronic properties have potential applications in sensors, solar cells, photocatalysis, optoelectronic devices, and biological imaging. Zinc oxide (ZnO) is an n-type II–IV semiconductor with high exciton binding energy (60 meV), high chemical and physical stability and wide band gap (3.37 eV). Due to these attractive physical properties it has found interesting applications in optics, and photoelectronic piezoelectric gas sensors. ZnO QDs are also *n*-type semiconductor because of intrinsic defects such as zinc interstitials and oxygen vacancies. Low costly and non-toxicity properties of ZnO QDs make them predominant for practical applications over other semiconductor quantum dots. The fabrication of semiconductor QDs nanodevices with high efficiency requires a deep understanding of the optoelectronic behavior of QDs, which depend on their impurity, size and shape. Many research works have been shown that the optical and electrical properties of ZnO QDs can be modified by ionic doping of suitable elements. The ZnO QDs have been vastly doped and co-doped with metals such as (Al, Ga, In, etc.) through different preparation techniques. It was found that the optical and electrical properties of ZnO QDs have increased as a result of doping [1–3]. Recently, rare-earth ions such as Ce^{3+}, Er^{3+}, Eu^{3+}, La^{3+}, Tb^{3+}, Tm^{3+}, Yb^{3+} and Dy^{3+} doped ZnO QDs have attracted the attention of scientific community [4–10]. Their unique optical properties and their 4f intra shell transitions give very intense emission peaks in the visible and near IR range. For example, the emission at wavelength of 1.55 nm by Er doped ZnO QDs make it possible to apply this component for optical communication technology [11,12]. ZnO has been selected as host for rare-earth elements not only because of its wide band gap that can be applicable for excitation of these elements, but also for its electrical conductivity [13–16]. So far, many techniques have been applied to produce rare-earth doped ZnO nanostructures such as co-deposition following evaporation, sintering, laser ablation and etec [17–23]. However, the mentioned methods are expensive and not efficient for producing rare-earth doped ZnO

*Corresponding author. Tel.: +351 916759671.
E-mail address: zamiri.r@gmail.com (R. Zamiri).

0272-8842/$ - see front matter © 2013 Elsevier Ltd and Techna Group S.r.l. All rights reserved.
http://dx.doi.org/10.1016/j.ceramint.2013.06.034

nanostructures because of the dopant might precipitate from the surface of ZnO nanocrystals due to the compact hexagonal wurtzite structure and high surface-to-volume ratio of ZnO nanocrystals.

In this paper a template-free precipitation method was used to prepare rare-earth doped ZnO nano powders. The aim of this study was to investigate the effects of rare-earth dopants on morphology and band gap of the prepared ZnO nanostructures.

2. Experimental procedure

Rare-earth doped ZnO nanocrystals were prepared by wet chemical precipitation. Firstly, 3.352 g of $ZnCl_2$ (Aldrich, Germany) and 2 mol% of each doping rare-earth element precursor, $(Er(NO_3)_3 \cdot 6H_2O$, $La(NO_3)_3 \cdot 6H_2O$ and $Yb(NO_3)_3 \cdot 6H_2O)$ were dissolved in distilled water. Each of the as obtained solution was dropped into 100 mL of 0.1 M NaOH (Merk, Germany) solution. The pH value of all the samples was around 13 and the precipitated materials were ultra-centrifuged (10,000 rpm, 10 min) to obtain clear supernatant liquids and washed with distilled water to remove the unwanted ions (Na^+, Cl^-, NO_3^-). This procedure was repeated several times up to getting a Na^+ concentration below to 0.66 ppm measured by atomic absorption spectroscopy, followed by drying at 80 °C for 24 h. The dried powders were then heat treated at 275 °C for 2 h. The chemical reactions that occurred during preparation were as follows:

$$ZnCl_2+2NaOH \rightarrow Zn(OH)_2+2NaCl \quad (1)$$

$$Zn(OH)_2 \rightarrow ZnO+H_2O \quad (2)$$

$$M(NO_3)_3+3NaOH \rightarrow M(OH)_3+3NaNO_3 \quad (3)$$

$$M(OH)_3 \rightarrow M_2O_3+3H_2O \quad (4)$$

M=Er, Yb and La

The experimental conditions for pure and rare-earth doped ZnO nanostructures were always kept constant along the present study, namely the type of solvent, precipitating agent (OH^-) and annealing temperature.

The structure and morphology of the samples were studied by X-ray diffraction (Shimadzu XRD-6000, Tokyo, Japan) and Scanning Electron Microscopy (SEM). The optical properties of the samples were carried out by Raman spectrometry and UV–vis Scanning Spectrophotometry (Perkin-Elmer, Lambda 35), which was equipped with a diffuse reflectance accessory.

3. Results and discussion

Fig. 1 shows the XRD diffraction patterns of undoped and rare earth doped (La, Yb and Er) ZnO nano powders. Well crystalline hexagonal structure without any diffraction peaks of a secondary phase or any impurity phase can be seen from spectra. All diffraction peaks are consistent with previously reported data for ZnO with lattice constant parameter of $a=3.24$ Å and $c=5.20$ Å (JCPDS 36-1451). This suggests that most of the rare earth ions might have been incorporated

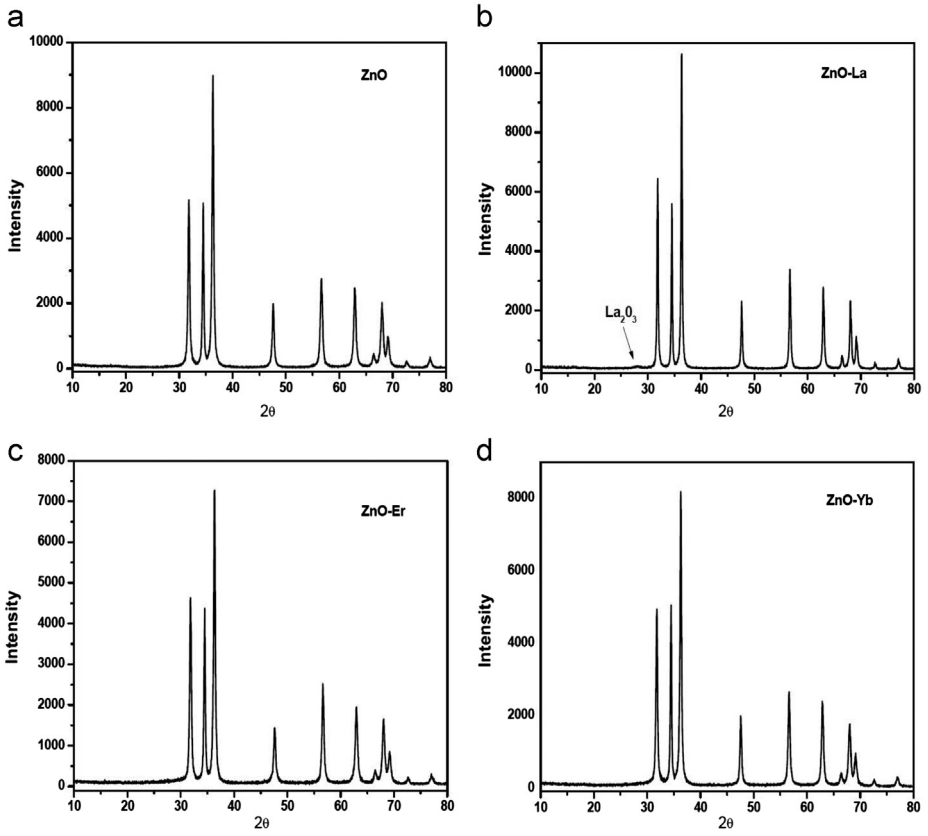

Fig. 1. XRD patterns of pure and rare-earth doped ZnO nano powders.

in the Zn^{2+} sites of the ZnO lattice. However, in the case of La-doped ZnO, a low intensity diffraction peak related to La_2O_3 appeared. The formation of La_2O_3 can be explained by the hindered incorporation of La in ZnO host due to the large difference between the radii of La^{3+} (1.15 Å) and Zn^{2+} ion (0.74 Å). This can be also inferred from the SEM micrograph (Fig. 2c) that shows different morphology clusters adhered to the ZnO nanorods, probably consisting of La_2O_3. In addition, although all the samples have similar diffraction patterns, it is possible to observe in Fig. 1 that the intensity of the peaks varied with different dopants, indicating differences in crystallinity. The intensity of the diffraction peaks decreased after doping with Yb and Er, indicating that crystallinity of the powders has also decreased. This can be understood considering the larger ionic radii of Yb^{3+} (0.86 Å) and Er^{3+}(0.89 Å) in comparison to that of Zn^{2+} (0.74 Å), which makes the replacement more and more difficult, thus distorting the ZnO lattice [24–26].

Fig. 2 presents the SEM images of pure and rare-earth doped ZnO nanostructures along with their corresponding EDS analysis. Different morphologies can be observed depending on the dopant ion incorporated. The obtained EDS results confirmed the presence of Er, La and Yb in the final products. The absence of extra peaks, besides the expectable ones in nanocrystals, suggests that the obtained products are very pure. Hedgehog's spikes like nanorods have been obtained for pure

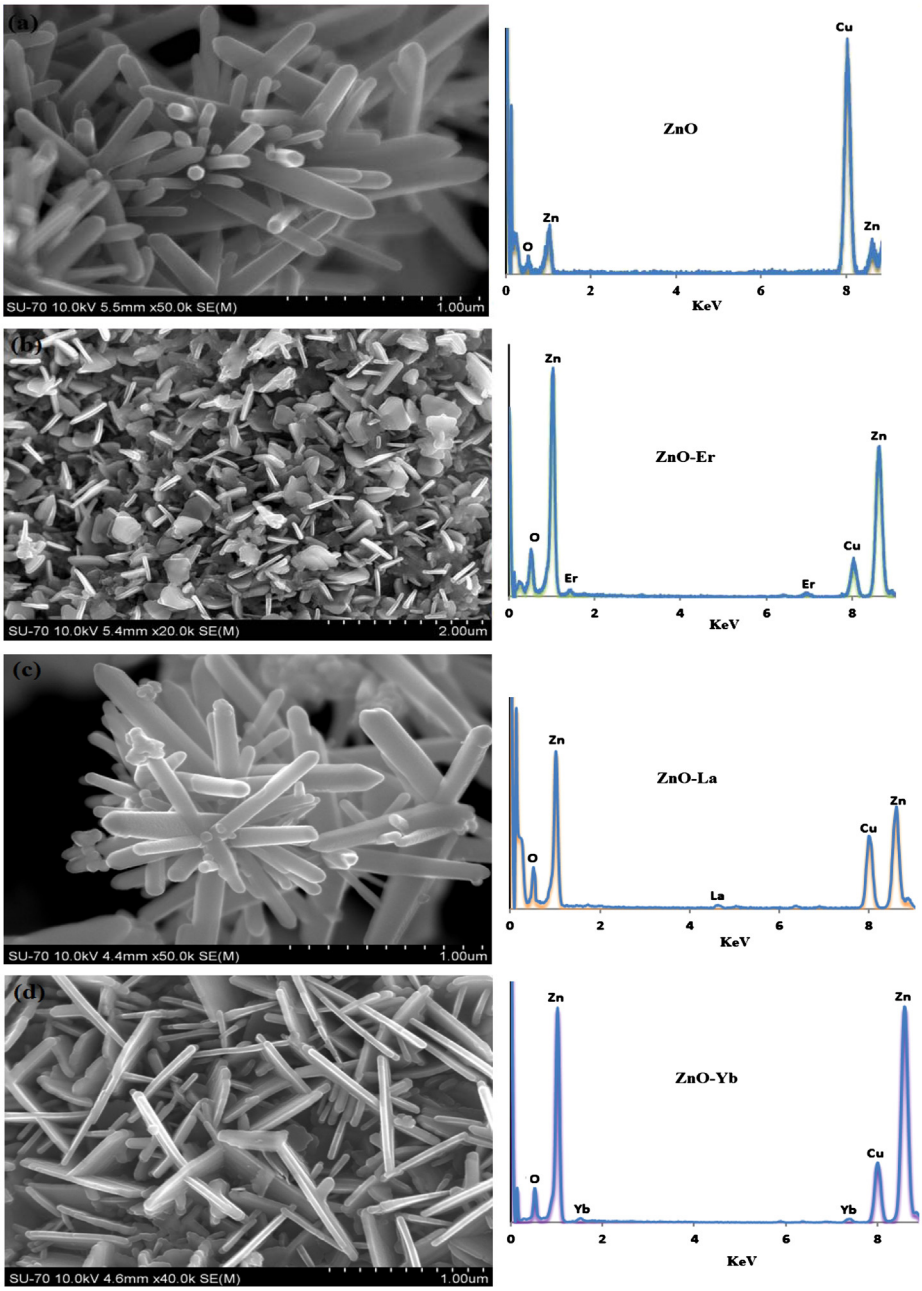

Fig. 2. SEM images of pure and rare-earth doped ZnO nanocrystals.

and La-doped ZnO, but in La-doped ZnO it can be seen that the elongated particles appear more agglomerated and intercrossed, while a few smaller and more isometric particles can be seen attached to the top of the rods. This last feature might be attributed to the precipitation of La_2O_3 in the final product. The almost similar morphologies obtained for pure and La-doped ZnO samples strongly suggest that the ZnO lattice was not much disturbed by the La ions, because their large size does not fit in the Zn lattice sites.

Doping of ZnO with Er and Yb remarkably changed the morphology of the nanostructures from nanorod-like to nanoplate-like. These morphological changes cannot be attributed to variation in the precipitating conditions, as they were kept constant to avoid any influence on the nucleation and crystal growth processes, and on the morphology of precipitated crystals. Therefore, the observed changes can only be attributed to the effects of dopants, which might act as structure driving agents through selectively adsorbing onto ZnO crystalline planes.

Structurally, ZnO has three types of crystalline planes, two non-polar $(2\bar{1}\bar{1}0)$ and $(01\bar{1}0)$ planes and a polar (0001) basal plane with C_{6V} symmetry. The (0001) plane has higher surface energy and therefore the growth of crystal in *c*-axis direction is faster which leads to the formation of nanorod shape crystals as it is indicated in Fig. 3a. No change in morphology was observed in the case of La-doped sample. However, a drastic change from nanorod-like to nanoplate-like occurred upon doping ZnO with Er and Yb (Fig. 3b). According to several literature reports, the (0001) surfaces of ZnO with tetrahedral structure usually expose terminal OH^- ligands to the solution [27,28]. The presence of the three valence ions instead of Zn^{2+} ions in the ZnO crystal is likely to enhance the adsorption of OH^- ligands onto these basal surfaces. These ligands will prevent further extensive deposition of Zn species at that surfaces leading

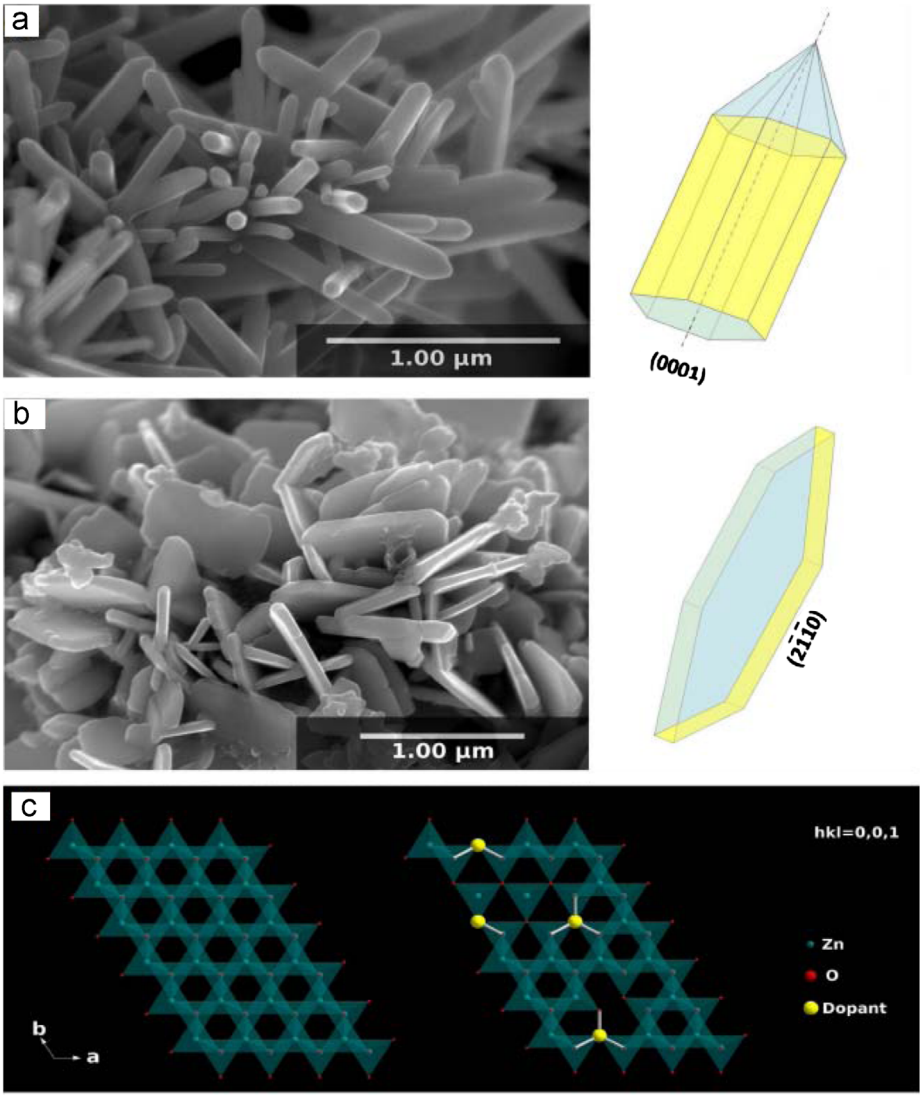

Fig.3. SEM images along with schematic crystal growth of (a) pure and (b) and Yb doped ZnO nanostructures. (c) Schematic crystal disturbance and growth in lateral directions after doping.

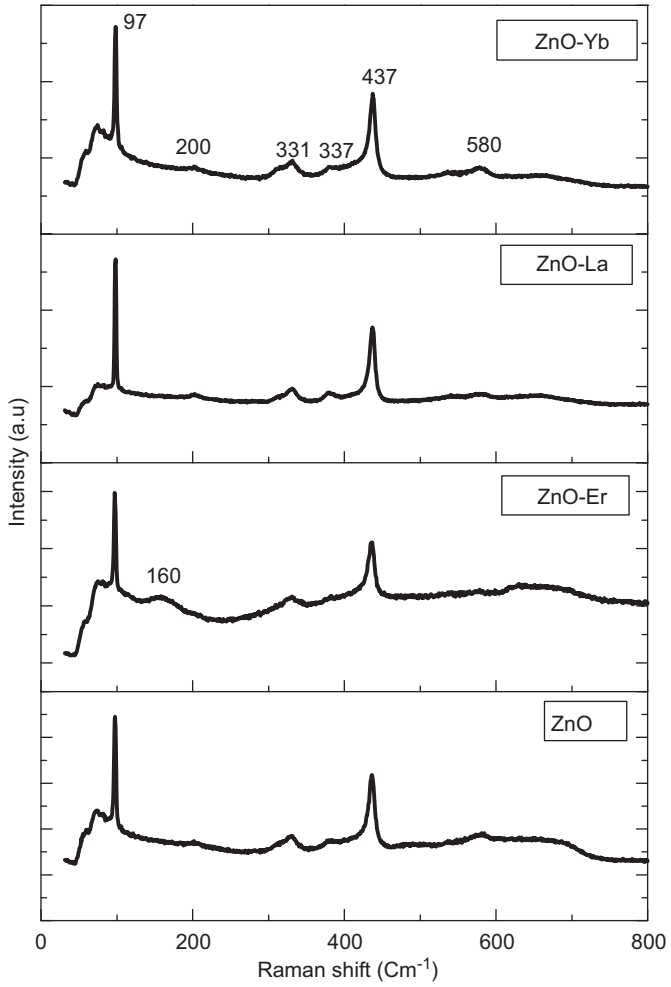

Fig. 4. Raman spectra of pure and rare-earth doped ZnO nanostructure powders.

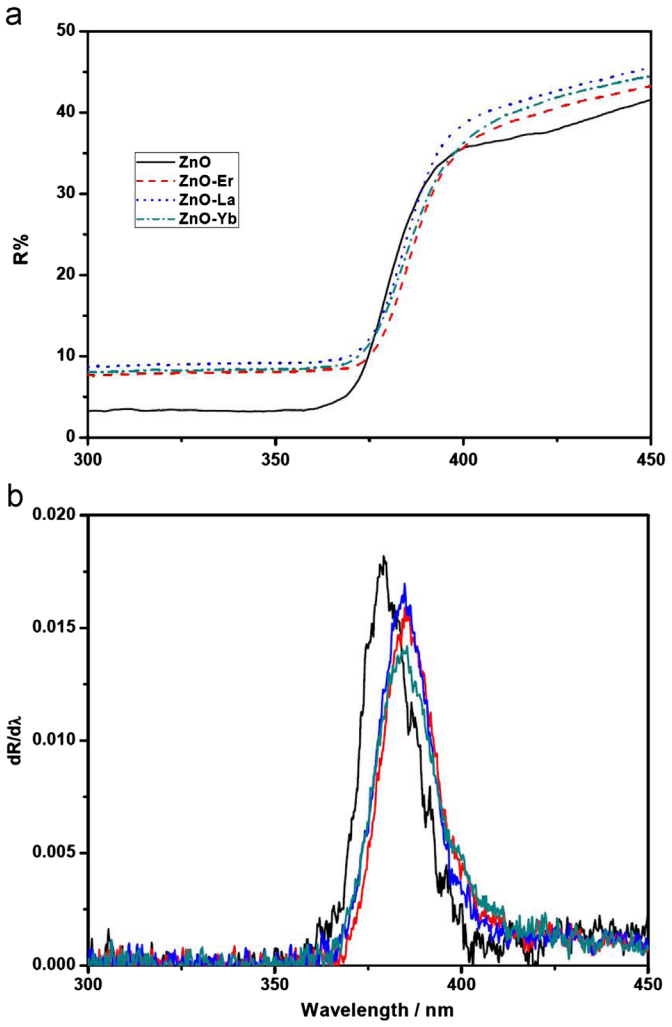

Fig. 5. (a) Diffuse reflectance spectrum of pure and rare-earth doped ZnO nano powders, and (b) the first derivative of diffuse reflectance as a function of wavelength.

Table 1
Phonon modes of all the prepared samples and of typical wurtzite single-crystal ZnO.

Sample	Single ZnO crystal	ZnO	ZnO–La	ZnO–Yb	ZnO–Er
E2 (low)	101, 102, 98	98	98	98	97
E2 (high)	437, 437.5, 441	436	437	437	437
A1 (TO)	378, 779, 380, 381	377	377	377	377
2-TA (M)	208	200	200	200	199
A1 (LO)	574, 576	580	580	580	580
2-E2 (MO)	332	331	331	331	331

Table 2
The calculated band gap values for pure and rare-earth doped ZnO nano powders.

Sample	Band gap	Shape
ZnO	3.26	Nanorod
ZnO–La	3.22	Nanorod
ZnO–Yb	3.21	Nanoplate
ZnO–Er	3.21	Nanoplate

to a decreased growth rate of ZnO nanocrystallites along the *c*-axis direction. This means that the crystal growth along the (0001) direction is significantly suppressed under this condition, whereas the nanocrystallites can still grow sideways along the $(2\bar{1}\bar{1}0)$ directions. Schematic of crystal structure disturbance of ZnO lattice with doping has been shown in Fig. 3c which shows crystal growth oriented along lateral directions.

The drastic morphological changes observed for the Er-doped and Yb-doped ZnO samples can therefore be regarded as a proof of the incorporation of these elements in the ZnO lattice.

Fig. 4 presents the Raman scattering signals for pure and doped ZnO powders excited by 532 nm laser. The Raman spectra of all samples are almost similar and the observed peaks can be assigned to the optical phonon modes of ZnO wurtzite crystal structure [29]. The ZnO with wurtzite crystal structure belongs to the space group of $^4C_{6V}$ ($P6_3mc$). There

are 4 atoms for each unit cell which lead to 12 phonon branches (9 optical and 3 acoustic), and according to group theory, the following modes can be predicted for optical modes [30–32]:

T=A1+2B1+E1+2E2.

There are two silent B1 modes, one E1 branch, one A1 branch and two E2 branches. The E1 and A1 are both infrared-active and Raman-active, while E2 is only Raman-active. Among these phonons, E1 and A1 have polar symmetry, and therefore A1 and E1 branches split into transverse optical (TO) and longitudinal optical (LO) components. As it was discussed earlier, the XRD analysis of the prepared nanostructures confirmed that all the samples possess hexagonal wurtzite structure. Therefore, as it is expected and confirmed by Raman scattering measurements, that all the samples present similar phonon responses. According to the literature [33], the peaks at 98, 377, 437 and 580 cm^{-1} can be assigned to E2 (low), A1 (TO), E2 (high) and A1 (LO), respectively. On the other hand, the peaks at 200 and 331 cm^{-1} are second-order phonons associated with the second-order Raman spectrum due to the M point phonons 2-TA (M), and 2-E2 (M), respectively. In comparison with pure ZnO nanorods, the Er-doped ZnO nanoplates exhibit an extra peak at 160 cm^{-1}. It is possible that the incorporation of Er^{3+} into the ZnO lattice produced internal strain and defects that activated this mode. In addition, the very sharp E2 (low) and E2 (high) peaks observed for all the samples (Fig. 4) further confirm that they have good crystal quality in agreement with XRD results. The nonpolar phonon modes with E2 symmetry have two frequencies, E2 (high) and E2 (low) related to Zn sublattice and oxygen atoms [33]. The phonon modes of all samples and of typical ZnO wurtzite single-crystal are listed in Table 1. Optical properties of nanomaterials are totally different from their bulk counterparts mainly due to the increase of surface-to-volume ratio, special spatial structures and drastic changes in electronic structure. However, as it can be seen from Table 1, the prepared nanostructures have almost the same phonon resonance in comparison with ZnO bulk single-crystal. This might be due to the much larger dimensions of the prepared nano particles when compared with ZnO Bohr radius (2 nm).

The UV–vis reflectance spectrums of samples are presented in Fig. 5a. A sudden decrease of reflectance intensity at a wavelength around 380 nm can be observed in all the samples and a red shift at the same wavelength can be observed in the rare earth doped ZnO powders. Band gap of semiconductor material can be estimated through the maximum value of the plot of the differential reflectance $dR/d\lambda$ versus λ (Fig. 5b) [34]. The obtained values of band gap are listed in Table 2. It was found that the Eg value for all the samples is smaller than that of the Eg value for pure ZnO (3.26 eV). This might be due to lower defect concentration in the crystals of pure ZnO. Interestingly, it can be seen that the Eg values are also dependent on the shape of structure. When La was used as a dopant the rod structure shape with the Eg value of 3.22 eV was obtained but in the case of Yb and Er dopants the structure shape is plate-like with Eg value of 3.21 eV. According to literature [35], ZnO particles with different shapes have different crystalline defect contents, which have impact on Eg values. This might be due to the electronic transition from the filled valence band to energy levels of defects instead of the electronic transition from the filled valence band to the empty conduction band which usually happens. In this sense, it is reasonable to conclude that the substitution of Zn site by rare-earth ions in ZnO crystal structure (as for Er and Yb) lead to a plate-like structure with higher amount of defects and smaller Eg values.

4. Conclusions

Pure and rare earth (La-, Er- and Yb-) doped ZnO nano powders were successfully prepared by wet precipitation. XRD analysis showed that La^{3+}ion cannot be easily incorporated into the ZnO crystal structure due to its large ionic size while $Er^{3+}$and Yb^{3+} enter well in the lattice to replace Zn^{2+}. SEM images showed that the incorporation of rare-earth ions in crystal structure of ZnO can drastically change the morphology of ZnO nano particles from nanorod-like to nanoplate-like. This morphological change could be explained by a decrease of ZnO crystal growth rate along vertical direction due to incorporation of Er^{3+} and Yb^{3+}ions in its crystal structure. Band gap value of pure ZnO has also changed due to defects produced with rare-earth doping.

Acknowledgments

The author Reza Zamiri would like to express his personal thanks to FCT (Fundação para a Ciência e a Tecnologia) for post-doctoral research grant with reference number (SFRH/BPD/76185/2011).

References

[1] G. Srinivasan, R.T. Rajendra Kumar, J. Kumar, Influence of Al doping on microstructure and optical properties of ZnO films prepared by sol–gel spin coating method, Optical Materials 30 (2007) 314–317.
[2] E.J.L. Arredondo, A. Maldonado, R. Asomoza, D.R. Acosta, M.A. M. Lira, M. de la, L. Olvera, Indium-Doped ZnO thin films deposited by the sol–gel technique, Thin Solid Films 490 (2005) 132–136.
[3] V. Fathollahi, M.M. Amini, Sol–gel preparation of highly oriented gallium-doped zinc oxide thin films, Materials Letters 50 (2001) 235–239.
[4] S. Liu, F. Liu, Z. Wang, Relaxation of carriers in terbium-doped ZnO nanoparticles, Chemical Physics Letters 343 (2005) 489–492.
[5] R.N Bhargava, V. Chhabra, T. Som, A. Ekimov, N. Taskar, Quantum confined atoms of doped ZnO nanocrystals, Physica Status Solidi B 229 (2002) 897–901.
[6] V. Chhabra, B.S. Kulkarni, R.N. Bhargava, 2000, US Patent No 6,036,886.
[7] F. Gu, S.F. Wang, M.K. Lu, G.Z. Zhou, D. Xu, D.R. Yuan, Photo-luminescence properties of SnO_2 nanoparticles synthesized by sol–gel method, Langmuir 20 (2004) 3528–3531.
[8] T. Schmidt, G. Muller, L. Spanhel, Activation of 1.54 μm Er^{3+} fluorescence in concentrated II–VI semiconductor cluster environments, Chemistry of Materials 10 (1998) 65–67.
[9] X. Wang, X. Kong, G. Shan, Y. Yu, Y. Sun, L. Feng, K. Chao, S. Lu, Y. Li, Luminescence spectroscopy and visible upconversion properties

of Er^{3+} in ZnO nanocrystals, Journal of Physical Chemistry B 108 (2004) 18408–18413.
[10] A. Ishizumi, Y. Kanemitsu, Structural and luminescence properties of Eu-doped ZnO nanorods fabricated by a microemulsion method, Applied Physics Letters 86 (2005) 253106–253109.
[11] S. Gao, H. Zhang, R. Deng, X. Wang, D. Sun, G. Zheng, Ballisticity of nanotube field-effect transistors: role of phonon energy and gate bias, Applied Physics Letters 89 (2006) 23125–23128.
[12] K. Takahei, A. Taguchi, Selective formation of an efficient Er–O luminescence center in GaAs by metalorganic chemical vapor deposition under an atmosphere containing oxygen, Journal of Applied Physics 74 (1993) 1979–1983.
[13] A. Polman, Erbium implanted thin film photonic materials, Journal of Applied Physics 82 (1997) 1–39.
[14] N. Mais, J.P. Reithmaier, A. Forchel, M. Kohls, L. Spanhel, G. Muller, Er doped nanocrystalline ZnO planar waveguide structures for 1.55 μm amplifier applications, Applied Physics Letters 75 (1999) 2005–2008.
[15] S. Komuro, T. Katsumata, T. Morikawa, X.W. Zhao, H. Isshiki, Y. Aoyagi, Highly erbium-doped zinc-oxide thin film prepared by laser ablation and its 1.54 μm emission dynamics, Journal of Applied Physics 88 (2000) 7129–7137.
[16] M. Ishii, S. Komuro, T. Morikawa, Y. Aoyagi, Local structure analysis of an optically active center in Er-doped ZnO thin film, Journal of Applied Physics 89 (2001) 3679 3675.
[17] J.H. He, C.S. Lao, L.J. Chen, D. Davidovic, Z.L. Wang, Large-scale Ni-doped ZnO nanowire arrays and electrical and optical properties, Journal of the American Chemical Society 127 (2005) 16376–16377.
[18] S. Bachir, K. Azuma, J. Kossanyi, P. Valat, J.C. Ronfard Haret, Photoluminescence of polycrystalline zinc oxide co-activated with trivalent rare earth ions and lithium. Insertion of rare-earth ions into zinc oxide, Journal of Luminescence 75 (1997) 35–49.
[19] Y.K. Park, J.I. Han, M.G. Kwak, H. Yang, S.H. Ju, W.S. Cho, Effect of coupling structure of Eu on the photoluminescent characteristics for ZnO: $EuCl_3$ phosphors, Applied Physics Letters 72 (1998) 668–671.
[20] S. Komuro, T. Katsumata, T. Morikawa, X. Zhao, H. Isshiki, Y. Aoyagi, 1.54 μm emission dynamics of erbium-doped zinc-oxide thin films, Applied Physics Letters 76 (2000) 3935–3938.
[21] X.T. Zhang, Y.C. Liu, J.G. Ma, Y.M. Lu, D.Z. Shen, W. Xu, G.Z. Zhong, X.W. Fan, Room-temperature blue luminescence from ZnO:Er thin films, Thin Solid Films 413 (2002) 257–261.
[22] P. Baviskar, P.R. Nikam, S.S. Gargote, A. Ennaoui, B.R. Sankapal, Controlled synthesis of ZnO nanostructures with assorted morphologies via simple solution chemistry, Journal of Alloys and Compounds 551 (2013) 233–242.
[23] P.P. Pal, J. Manam, Structural and photoluminescence studies of Eu^{3+} doped zinc oxide nanorods prepared by precipitation method, Journal of Rare Earths 31 (2013) 37–43.
[24] C. Bingqiang, C. Weiping, From ZnO nanorods to nanoplates: chemical bath deposition growth and surface-related emissions, Journal of Physical Chemistry C 112 (2008) 680–685.
[25] C. Dewei, L. Sean, Growth and electrical properties of doped ZnO by electrochemical deposition, New Journal of Glass and Ceramics 2 (2012) 13–16.
[26] Z. Jun, S. Lingdong, Y. Jialu, S. Huilan, L. Chunsheng, Y. Chunhua, Control of ZnO morphology via a simple solution route, Chemistry of Materials 14 (2002) 4172–4177.
[27] J Slunecko, M. Kosec, Morphology and crystallization behavior of sol–gel-derived titania, Journal of the American Ceramic Society 81 (1998) 1121–1133.
[28] P.K. Dutta, P.K Gallagher, Raman spectroscopic and thermoanalytical studies of the reaction of barium hydroxide with anatase and titanium oxide gels, Journal of Materials Chemistry 4 (1992) 847–851.
[29] U. Pal, J.G. Serrano, P. Santiago, G. Xiong, K.B. Ucer, R.T. Williams, Synthesis and optical properties of ZnO nanostructures with different morphologies, Optical Materials 29 (2006) 65–69.
[30] F. Decremps, J.P Porres, A.M Saitta, J.C Chervin, A. Polian, High-pressure Raman spectroscopy study of wurtzite ZnO, Physical Review B 65 (2002) 092101–092104.
[31] J.M. Calleja, M. Cardona, Resonant Raman scattering in ZnO, Physical Review B 16 (1977) 3753–3761.
[32] R. Loudon, The Raman effect in crystals, Advances in Physics 13 (1964) 423–482.
[33] M. Rajalakshmi, A.K. Arora, B.S Bendre, S. Mahamuni, Optical phonon confinement in zinc oxide nanoparticles, Journal of Applied Physics 87 (2000) 2445–2448.
[34] M. Radecka, M. Rekas, K. Zakrzewska, Titanium dioxide in photoelectrolysis of water, Trends in Inorganic Chemistry 9 (2006) 81–126.
[35] S. Suwanboona, P. Amornpitoksukb, P. Bangrakc, A. Sukolratd, N. Muensite, The dependence of optical properties on the morphology and defects of nanocrystalline ZnO powders and their antibacterial activity, Journal of Ceramic Processing Research 11 (2010) 547–551.